Annals of Circulation

Kuzyk Yu.I.[1]*, Ivanov D.V.[2] and Dol A.V.[2]

[1]Danylo Halytsky Lviv National Medical University, Ukraine
[2]Education and Research Institute of Nanostructures and Bio Systems of Saratov State University, Russia

Dates: **Received:** 15 March, 2016; **Accepted:** 15 April, 2016; **Published:** 19 April, 2016

***Corresponding author:** Yulia Kuzyk, Danylo Halytsky Lviv National Medical University, Ukraine, E-mail: juliakuzyk@mail.ru

www.peertechz.com

Keywords: Carotid artery; Atherosclerosis; Biomechanics; Plaques

Research Article

Biomechanical Bases of Forecasting Occurrence of Carotid Atherosclerosis

Abstract

The purpose of this study was to investigate changes of the effective and shear stresses level on the surface of atherosclerotic plaques in comparison with the healthy vessel wall, as well as distribution of the hemodynamic forces. Two software modules were used: ANSYS CFX for simulating blood flow, and Structural (Mechanical) for simulating the stress-strain state of the walls. Geometric models of vessels were built on basis of healthy and diseased vessels casts in the CAD system SolidWorks. We discovered the phenomenon of stress-strain state of atherosclerotic plaques: soft plaque is different from the rigid, which creates conditions for plaque rupture under the influence of blood pressure and shear stress. The stress difference between rigid and unchanged vessel with carotid stenosis creates additional flows and vortexes, growing in proportion to the increase of the plaque size. In addition, such state can be directly related to the development of mural thrombosis. Analysis of the blood flow velocities vector field and pattern of streamlines in the external carotid artery demonstrates a complete blockage of the vessel. Vortex and congestion area formation in the ampoule of internal carotid artery creates conditions for further plaque progression.

Introduction

Damage of the endothelium in response to hemodynamic stress is a major issue in the development of atherosclerosis disease (AD). Wall shear stress (WSS) is one of the most significant mechanical factors affecting on AD appearance [1-3]. Scientists [4-7], are used to associate WSS with intimal hyperplasia of the vascular wall.

High shear stresses can cause damage to the endothelial layer of the wall, activation and aggregation of platelets, formation of thrombosis [8,9] and plaque rupture [10].

In present time most researchers considered low wall shear stress is directly associated with AD [3, 4, 10-13]. Younis [14], notes that the wall shear stresses below 1.5 Pa stimulating atherogenic phenotype and is usually seen in areas prone to atherosclerotic deposits. Particular geometries in the arteries, such as bifurcations, bindings and anastomoses can create focal areas of reduced wall shear stress and stimulate the proliferation of smooth muscle cells. The most specific area of wall shear stress localized significant reduction is a bifurcation of the carotid artery [15]. A feature of the carotid bifurcation is the presence of sinus in the first segment of the internal carotid artery (ICA). This local extension of the lumen with a branch and various outflow resistance in the internal and external carotid arteries leads to the formation of a complex flow system. Flow separation occurs along the outer wall of the ICA sinus situated opposite the flow divider, and leads to velocity profile offset toward the inner wall of the ICA. These characteristics of the flow conduct the formation of large areas of low shear stress along the outer wall of the carotid artery. They also lead to the reverse flow periods within each pulse cycle formation. The highest value of the effective stress is detected in the apex of the bifurcation. It is in this section the blood flow is dividing, causing such stress state.

Effective stress in the wall is another mechanical factor affecting on the vessel, causing the weakening of the wall and subsequent development of atherosclerotic deposits. Therefore, this area of the carotid bifurcation has the tendency to AD and different proliferative processes development. On the contrary, the inner wall of the carotid bifurcation has a higher wall shear stress and the blood flow is unidirectional, and so at this location there is less intimal thickening and atherosclerotic plaques (AP) appearing. Thus, proliferating intimal thickening developing focally in those areas where the geometric features change the blood flow to reduce wall shear stress. Tang [9], concluded that both low and high shear stresses lead to the formation of thrombosis. There is an opinion [16], that AD arises because of fatigue in the areas of stress concentration. It is assumed that the AD localization explained by changes in the wall shear stresses and equivalent stress in the vessel wall [17,18].

One can assume that the changes in the level of effective and shear stresses in conjunction with the level of oscillating stress may be used as a criterion for predicting the behaviour of different AP types.

Purpose

The purpose of this study was to investigate changes of the effective and shear stresses level on the surface of atherosclerotic plaques in comparison with the healthy vessel wall, as well as distribution of the hemodynamic forces.

Materials and Methods

In this paper the fluid-structure interaction problems were solved. In the simulation, it was assumed that the blood is incompressible, homogeneous viscous Newtonian fluid, and the blood flow is described by the Navier-Stokes equations [19].

The closed system of Navier-Stokes equations (three equations of motion and the continuity equation) is as follows:

$$\tilde{n}\left(\frac{\partial v_i}{\partial t}+\frac{\partial v_i}{\partial x_j}v_j\right)=f_i-\frac{\partial p}{\partial x_i}+\grave{i}\nabla^2 v_i,$$

$$\overline{v}$$

$$0,$$

$$div$$

Where $\nabla^2=\frac{\partial^2}{\partial x_i{}^2}$ - Laplace operator in the Cartesian coordinate system.

This system can be written in vector form:

$$\frac{\partial\overline{v}}{\partial\tilde{n}}+(\frac{\overline{v}}{\tilde{n}}\cdot\nabla)\overline{v}=\frac{\overline{f}}{\tilde{n}}-\frac{1}{}gradp+\frac{\mu}{}\Delta\overline{v},\quad div\overline{v}=0,$$

Where $\nabla=\frac{\partial}{\partial x_i}\cdot\overline{e_i}$ - the Hamiltonian operator in the Cartesian basis.

Blood viscosity was assumed to be 0.004 Pa s and density was 1050 kg / m3. In [20], it was shown that the non-Newtonian blood properties must be taken into account only in the small vessels simulations (diameter less than 0.1 mm), when the flow velocity and the shear stresses are small. The wall was considered incompressible, isotropic, linearly elastic and homogeneous. Mechanical characteristics (Young's modulus and Poisson's ratio) of the wall and AP were taken from the literature [21].

The equations of motion for an elastic body movements satisfying Hooke's law in the case of small deformations are called Lame equations or the Navier-Lame. They are derived from the equations of continuous medium motion by substituting the expressions for components of stress tensor and components of small strains tensor $p_{ij}=\lambda I_1(\varepsilon)\delta_{ij}+2\mu\varepsilon_{ij},$, as well as the Cauchy equations linking components of the small deformations tensor and displacement vector components $\mathring{a}_{ij}=\frac{1}{2}\left(\frac{\partial u_i}{\partial x_j}+\frac{\partial u_j}{\partial x_i}\right)$. Where λ,μ are Lame elastic constants, $I_1(\varepsilon)$ is the first invariant of the small deformations tensor.

Lame equations are:

$$(\lambda+\mu)grad\ div\,\overline{u}+\mu\Delta\overline{u}+\rho\overline{F}=\rho\overline{a},$$

Where $\overline{a}$ - acceleration.

In a Cartesian coordinate system they can be written as follows:

$$\rho\,a_x=(\lambda+\mu)\frac{\partial}{\partial x}\left(\frac{\partial u}{\partial x}+\frac{\partial v}{\partial y}+\frac{\partial w}{\partial z}\right)+\mu\left(\frac{\partial^2 u}{\partial x^2}+\frac{\partial^2 u}{\partial y^2}+\frac{\partial^2 u}{\partial z^2}\right)+\rho F_x,$$

$$\rho\,a_y=(\lambda+\mu)\frac{\partial}{\partial y}\left(\frac{\partial u}{\partial x}+\frac{\partial v}{\partial y}+\frac{\partial w}{\partial z}\right)+\mu\left(\frac{\partial^2 v}{\partial x^2}+\frac{\partial^2 v}{\partial y^2}+\frac{\partial^2 v}{\partial z^2}\right)+\rho F_y,$$

$$\rho\,a_z=(\lambda+\mu)\frac{\partial}{\partial z}\left(\frac{\partial u}{\partial x}+\frac{\partial v}{\partial y}+\frac{\partial w}{\partial z}\right)+\mu\left(\frac{\partial^2 w}{\partial x^2}+\frac{\partial^2 w}{\partial y^2}+\frac{\partial^2 w}{\partial z^2}\right)+\rho F_z,$$

Where u, v, w are displacement vector components, and F_x, F_y. F_z - components of the external volume forces, which were not considered in this study?

The system of Lame equations for dynamic problem becomes closed, if we add the definition of acceleration

$$\overline{a}=\frac{d\overline{v}}{dt}=\frac{\partial\overline{v}}{\partial t}+v_i\frac{\partial\overline{v}}{\partial x_i},\overline{v}=\frac{d\overline{u}}{dt}.$$

Lame equations are derived under the condition of small deformations, but displacement, velocity and acceleration can be finite.

Solving basic system of equations [19], was carried out numerically using the finite element method in the finite element software ANSYS. Two software modules were used: ANSYS CFX for simulating blood flow, and Structural (Mechanical) for simulating the stress-strain state of the walls.

Geometric models of vessels were built on basis of healthy and diseased vessels casts in the CAD system SolidWorks. The carotid arteries were removed from cadavers during autopsies on the level of separation from aorta to the level of entry into the skull. Based on these vessels corrosive preparations (casts of the common carotid, internal and external carotid arteries) were made. Then they were imaged and outlined. Cross sections of healthy blood vessels considered circle. Figure 1 shows an image of a cast with cross-section of the internal lumen.

Next, the same method was used to create a geometric model of arterial wall. The wall of healthy blood vessels are also considered circular cross-section. Figure 2 shows the model of a healthy carotid artery.

During the simulation at the inlet of the common carotid artery linear time-dependent blood flow velocity was determined. The simulation was performed for two cardiac cycles within 2 seconds. Analysis of the results was held for a second cardiac cycle from 1 to 2 second.

For the AP analysis a model of carotid artery plaque in the area of the bifurcation area was created (Figure 3). The narrowing of the vessel lumen was 50% of the original diameter. This model was chosen because of the most frequent localization of the carotid AD in this area according to the literature [15].

Results and Discussion

AP configuration significantly reduced the rate of blood flow in the external carotid artery (ECA). Blood flow in the ECA is practically stopped after the bifurcation. This AP configuration leads to almost complete blockage of the vessel, both in systole and diastole (Figures 4,5).

Analysis of the streamlines is also confirms blocking of the ECA: there is no significant blood flow in vessel both in the case of soft and hard plaque (Figures 6,7). In addition, in the ICA ampoule in case of both soft and hard AP significant vortex flow and the formation of the congestion zone were observed. At this point there is a possibility to further formation and progression of AP.

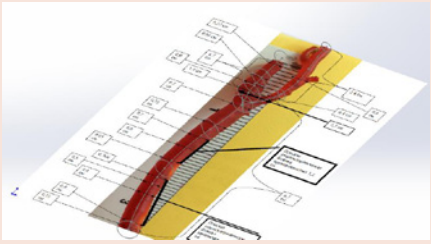

Figure 1: Cast of the carotid artery with cross-sections.

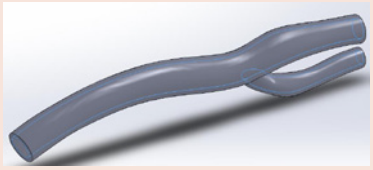

Figure 2: Model of healthy carotid artery.

Figure 3: Model of the vessel with the plaque in bifurcation area.

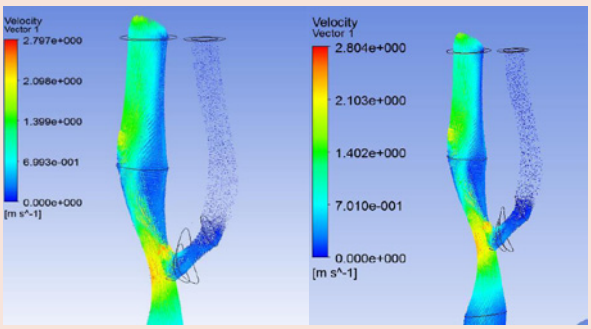

Figure 4: Velocity field in systole. Left – soft plaque, right – tough plaque.

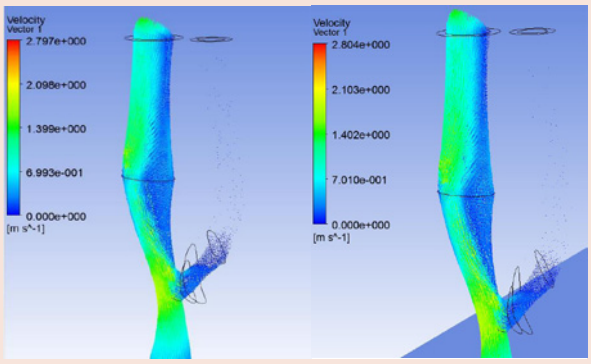

Figure 5: Velocity field in diastole. Left – soft plaque, right – tough plaque.

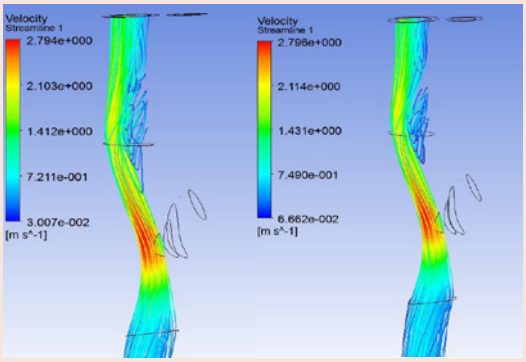

Figure 6: Streamlines (systole). Left – soft plaque, right – tough plaque.

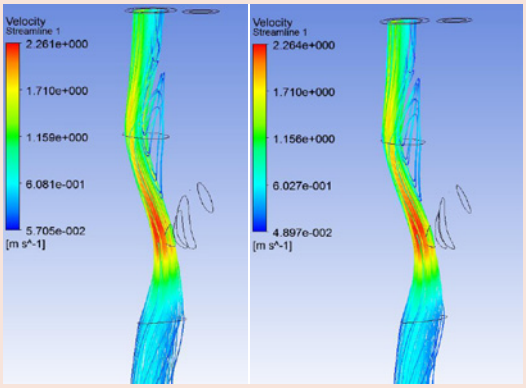

Figure 7: Streamlines (diastole). Left – soft plaque, right – tough plaque.

The maximum effective stress values were observed at the boundary between the healthy part of the common carotid artery (CCA) and the section with AP. In the case of soft plaque maximum values were much higher than in the case of hard plaque (Figure 8). This may cause soft plaque detachment and further thrombus formation. Meanwhile in the case of the soft plaque there is minimal stress in plaque itself, while a rigid plaque stress value order coincides with the maximum stress.

The lowest shear stresses both in the case of soft and tough plaques appeared on the inner wall of ICA on the site after the bifurcation junction (ampoule). ECA in this case was also subjected to a minimum shear stresses. This can be explained by the peculiarities of hemodynamic pattern: there was no active blood flow in the vessel. The highest shear stresses on AP were observed in apex bifurcation point. This is due to a significant narrowing of the artery in this area and the significant increase in the flow rate. A similar pattern was observed throughout the whole cardiac cycle with both types of AP (Figure 9).

Thus, for both types of plaques stress-strain state of the vessel matched in general. The highest stress occurs at boundary between the healthy part of the CCA and AD affected part. The lowest shear stresses observed in the ICA ampoule. The main difference is in the distribution of the effective stress on the plaque at the bifurcation node due to varying plaques hardness.

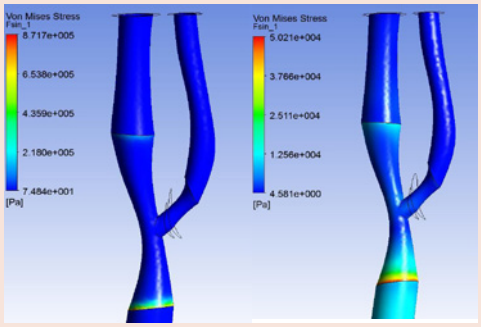

Figure 8: Effective stress in the wall near the bifurcation. Left – soft plaque, right – tough plaque.

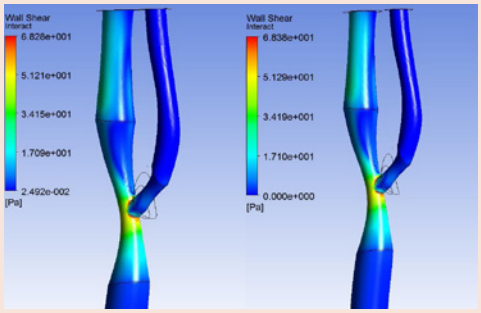

Figure 9: Wall shear stress. Left – soft plaque, right – tough plaque.

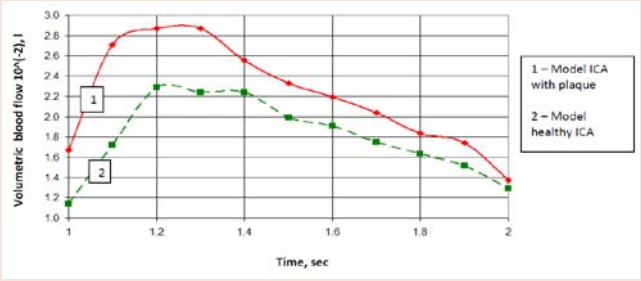

Figure 10: Volume flow at the outlet of ICA.

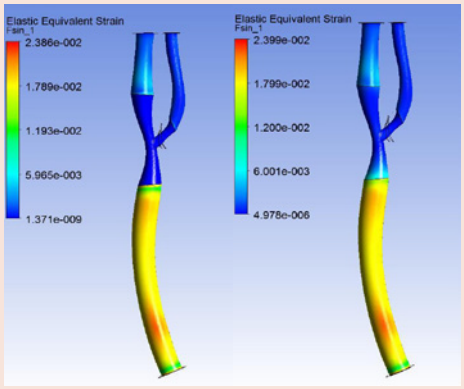

Figure 11: Deformations of the model with soft (left) and rigid (right) plaques.

In case of the affected vessel volume blood flow was very small at the outlet of the ECA. In case of the affected vessel there was almost 30% increasing of blood flow in ICA in comparison to healthy artery. This will certainly have a negative effect on the hemodynamics (Figure 10).

The distribution patterns of effective strain in the vessel wall with tough and soft plaques did not differ much. Strain orders are also coincided (Figure 11).

The maximum deformation was observed in the CCA, which is caused by geometric features of the AP. This feature may lead to a further weakening of the CCA wall and AD progression.

Anatomically realistic simulation of blood flow is important for understanding the role of hemodynamic factors in the development and prognosis of atherosclerotic disease. Studies have shown that the genesis and progression of atherosclerosis is directly correlated with the distribution of the hemodynamic forces and contributes to atherogenesis [4,9,22]. The mechanics of blood flow in the arteries of a person, the relationship between the geometry of the vessel and the progression of atherosclerotic plaques has been proven by various authors [3,8,14,17,19].

Our study proves once again the important role of hemodynamics and wall shear stress in the development and progression of carotid atherosclerosis. Our work complements and extends the idea of carotid atherosclerosis as the main risk factor for stroke. To date, the basic research carried out by means of computer modeling techniques based on ultrasonographic examination of the carotid arteries. Sousa L. et al., in their research presented a noninvasive approach for simultaneously quantifying subject-specific flow patterns and wall shear stress distributions of human carotid bifurcation using a combination of US data and computer fluid dynamics (CFD) modeling. Application of this approach to a normal volunteer and five subjects with atherosclerosis demonstrated WSS-based descriptors to be correlated and extremely sensitive to variation in geometry and able to capture flow disturbances due to stenotic plaques [23,24]. In their opinion, one interesting area for further research is to develop a diagnosis procedure incorporating medical video and 3D ultrasound images, because multiple views given by medical video allow an improved 3D reconstruction of the carotid artery [23,25]. Computer fluid dynamics based on ultrasonographic research is expected to contribute towards pathologic findings. Hemodynamic CFD parameters such as WSS are extremely important since plaque ulceration is related to the existence of high WSS at the upstream region of the plaque and on the contrary, regions exposed to low WSS are most prone to develop atherosclerotic plaques [23]. Surgical planning and therapy outcomes for atherosclerotic carotid bifurcation would benefit from a US based diagnosis assistance platform [26].

Another interesting approach is method of video segmentation of the carotid artery. This method may be used to estimate the motion, find and track the boundaries of the plaque, classifying the motion of the plaque in normal or abnormal, and thus finding normal and abnormal plaques. Since disturbed hemodynamics might be important in assessing the prognostic of further progression of the atherosclerotic disease, the hemodynamic modeling incorporating

non-rigid walls will be better suited at evaluating the tensile stresses within a vulnerable plaque. Subject specific identification of the link between hemodynamic behavior and stenosis pathophysiology might allow testing hypotheses and to address important clinical vascular problems, improving diagnostic and therapy treatment or surgical planning [27]. In contrast to the above work, we conducted studies on autopsy material, taken at autopsy of patients of different age groups. Production of corrosive carotid method allowed us to create a realistic anatomical model of the vessel, which allowed to carry out an objective atherogenesis modeling using finite element methods of forecasting (ANSYS). In the future we plan to expand the study due to application of the method ANSYS CFX in ultrasonographic research of the carotid arteries.

Conclusion

We discovered the phenomenon of stress-strain state of atherosclerotic plaques: soft plaque is different from the rigid, which creates conditions for plaque rupture under the influence of blood pressure and shear stress. The stress difference between rigid and unchanged vessel with carotid stenosis creates additional flows and vortexes, growing in proportion to the increase of the plaque size. In addition, such state can be directly related to the development of mural thrombosis. Analysis of the blood flow velocities vector field and pattern of streamlines in the external carotid artery demonstrates a complete blockage of the vessel. The increase of volume blood flow in ICA by about 30% leads to negative changes in hemodynamics and increased manifestations of cerebrovascular insufficiency. Vortex and congestion area formation in the ampoule of ICA creates conditions for further plaque progression. Increased level of effective stresses at the junction of the health sector and the vessel affected by atherosclerosis in the case of soft plaque creates the conditions for the plaque rupture and further thrombus formation.

The ultrasound data on the plaque structure can be used to predict future behaviour of different plaques types in the carotid atherosclerosis. Analysis of the distribution of hemodynamic forces shows weaknesses in the ampoule and bifurcation node of the carotid arteries, which should be considered during reconstructive surgery.

References

1. Purynya BA, Kasyanov VA (1980) Biomechanics of large blood vessels of human. Riga Zinatne 260.
2. Learoyd BM, Taylor MG (1966) Alterations with Age in the Viscoelastic Properties of Human Arterial Walls. Circ Res 18: 278–292.
3. Hyun S, Kleinstreuer C, Archie JP Jr. (2003) Computational analysis of effects of external carotid artery flow and occlusion on adverse carotid bifurcation hemodynamics. J Vasc Sur 37: 1248–1254.
4. Filipovic N, Kojic M (2004) Computer simulations of blood flow with mass transport through the carotid artery bifurcation. Theoret Appl Mech 31: 1–33.
5. Augst AD1, Ariff B, McG Thom SA, Xu XY, et al (2007) Analysis of complex flow and the relationship between blood pressure, wall shear stress, and intima-media thickness in the human carotid artery. J Physiol Heart Circ Physiol 293: 1031–1037.
6. Bonert M, Leask RL, Butany J, Ethier CR, Myers JG, et al. (2003) The relationship between wall shear stress distributions and intimal thickening in the human abdominal aorta. Biomed Eng Online 2: 18.
7. Joshi AK, Leask RL, Ojha M, Myers JG, Butany J, et al. (2003) Correlation of wall shear stress and intimal thickening in the right coronary artery. Summer Bioengineering Conference 1031–1032.
8. Birchall D1, Zaman A, Hacker J, Davies G, Mendelow D (2006) Analysis of haemodynamic disturbance in the atherosclerotic carotid artery using computational fluid dynamics. Eur Radiol 16: 1074–1083.
9. Tang D, Yang C, Ku DN (1999) A 3-D thin-wall model with fluid-structure interactions for blood flow in carotid arteries with symmetric and asymmetric stenoses. Computers and Structures 72: 357–377.
10. Tan FPP, Soloperto G, Wood NB, Thom S, Hughes A, et al. (2008) Advanced Computational Models for Disturbed and Turbulent Flow in Stenosed Human Carotid Artery Bifurcation. Biomed 21: 390–394.
11. Caro CG, Fitz-Gerald JM, Schroter RC (1971) Atheroma and Arterial Wall Shear Observation, Correlation and Proposal of a Shear Dependent Mass Transfer Mechanism for Atherogenesis. Proc R Soc Lond B Biol Sci 177: 109–159.
12. Caro CG (2009) Discovery of the Role of Wall Shear in Atherosclerosis. Arterioscler Thromb Vasc Biol 29: 158–161.
13. Martin D, Zaman A, Hacker J, Mendelow D, Birchall D (2009) Analysis of haemodynamic factors involved in carotid atherosclerosis using computational fluid dynamics. The British Journal of Radiology 82: 33–38.
14. Younis HF1, Kaazempur-Mofrad MR, Chung C, Chan RC, Kamm RD (2003) Computational analysis of the effects of exercise on hemodynamics in the carotid bifurcation. Ann Biomed Eng 31: 995–1006.
15. Kazanchyan PO, Valykov EA, Derzanov AV (2007) Surgical treatment of pathological deformations of the internal carotid arteries. Almanach of clinical medicine 73-76.
16. Thubrikar MJ (2007) Vascular mechanics and pathology. NY: Springer Science+Business Media 494.
17. Delfino A, Stergiopulos N, Moore JE Jr, Meister JJ (1997) Residual strain effects on the stress field in a thick wall finite-element model of the human carotid bifurcation. J Biomech 30: 777–786.
18. Salzar RS, Thubrikar MJ, Eppink RT (1995) Pressure-induced mechanical stress in the carotid artery bifurcation: a possible correlation to atherosclerosis. J Biomech 28: 1333–1340.
19. Ivanov D, Dol A, Pavlova O, Aristambekova A (2014) Modeling of human circle of Willis with and without aneurisms. Acta Bioeng Biomech 16: 121-129.
20. Ku JP, Elkins CJ, Taylor CA (2005) Comparison of CFD and MRI flow and velocities in an in vitro large artery bypass graft model. Ann Biomed Eng 33: 257-269.
21. Khamdaeng T, Luo J, Vappou J, Terdtoon P, Konofagou EE (2012) Arterial stiffness identification of the human carotid artery using the stress-strain relationship in vivo. Ultrasonics 52: 402-411.
22. Jodas DS, Pereira AS, Tavares JM (2016) A review of computational methods applied for identification and quantifications of atherosclerotic plaques in images. Expert System with Applications 46: 1-14.
23. Sousa LC, Castro CF, António CC, Santos AM, dos Santos RM, et al. (2014) Towards hemodynamic diagnosis of carotid artery stenosis based on ultra sound image data and computational modelling. Med Biol Eng Comput 51: 971-983.
24. Suosa LC, Castro CF, Antonio CAC, Tavares JMRS, Santos AMF, et al. (2014) Simulated hemodynamics in human carotid bifurcation based on Doppler ultrasound data. International Journal of Clinical Neurosciences and Mental Health 1: 14-21.
25. Suosa LC, Castro CF, Antonio CAC, Santos AMF, Santos RM (2014) Haemodynamic conditions of patient-specific carotid bifurcation based on ultrasound imaging. Computer Methods in Biomechanics and Biomedical Engineering: Imaging & Visualization 2: 157-166.
26. Suosa LC, Castro CF, Antonio CAC, Tavares JMRS, Santos AMF, et al.

(2013) Automatic segmentation of the lumen of the carotid artery in ultrasound B-mode images. SPIE Medical Imaging 2013, Proc. SPIE 8670, 16.

27. Santos AMF, dos Santos RM, Castro PMAC, Azevedo E, Suosa L, et al. (2013) A novel automatic algorithm for the segmentation of the lumen of the carotid artery in the ultrasound B-mode images. Expert System with Applications 40: 6570-6579.

28. Lawton RW (1954) The Thermoelastic Behavior of Isolated Aortic Strips of the Dog. Circ Res 2: 344–353.

29. Ivanov D (2009) Mechanical properties of Willis circle arteriesю CMM 2009. Short papers / ed. by Kuczma M, Wilmanski K, Szajna W, Zielona Gora 213-214.

30. Kirillova IV, Shchuchkina OA (2012) Physical and mechanical properties of the coronary arteries of the heart of human. Mathematical modeling and biomechanics in the modern university: Tez. rep. VII All-Russian school-seminar. Rostov-on-Don 69.

31. Tseders EE, Kasyanov VA (1978) Installation for the study of walls of blood vessels in the dynamic mode. Mechanics polymers 4: 745–747.

32. Khamin NS (1978) The strength properties of the human iliac and carotid arteries and their changes with age. Polymer Mechanics 14: 715–718.

33. Patel DJ, Janicki JS, Vaishnav RN, Young JT (1973) Dynamic anisotropic viscoelastic properties of the aorta in living dogs. Circ Res 32: 93–107.

34. Vaishnav RN, Young JT, Janicki JS, Patel DJ (1972) Nonlinear anisotropic elastic properties of the canine aorta. Biophys J 12: 1008–1027.

35. Rabotnov Yu H (1988) Mechanics of deformable solids. M 712.

36. Malek AM, Alper SL, Izumo S (1999) Hemodynamic shear stress and its role in atherosclerosis. JAMA 282: 2035-2042.

Citation: *Kuzyk YuI, Ivanov DV, Dol AV (2016) Biomechanical Bases of Forecasting Occurrence of Carotid Atherosclerosis. Ann Circ 1(1): 001-006.*